Probabilistic Harmonic Modeling of Wind Power Plants

Guest, Emerson; Jensen, Kim H.; Rasmussen, Tonny Wederberg

Published in:
Proceedings of 16th Wind Integration Workshop

Publication date:
2017

Document Version
Peer reviewed version

Probabilistic Harmonic Modeling of Wind Power Plants

Emerson Guest, Kim H. Jensen, and Tonny W. Rasmussen,

***Abstract*—A probabilistic sequence domain (SD) harmonic model of a grid-connected voltage-source converter is used to estimate harmonic emissions in a wind power plant (WPP) comprised of Type-IV wind turbines. The SD representation naturally partitioned converter generated voltage harmonics into those with deterministic phase and those with probabilistic phase. A case study performed on a string of ten 3MW, Type-IV wind turbines implemented in PSCAD was used to verify the probabilistic SD harmonic model. The probabilistic SD harmonic model can be employed in the planning phase of WPP projects to assess harmonic emissions to a given quantile, potentially avoiding an over-engineering of passive filters otherwise needed to satisfy infrequently occurring cases.**

I. Introduction

The computation of power quality (PQ) of grid-connected power-electronic devices is an ongoing area of research for the energy industry [1]. An estimation of harmonic emissions is usually performed in the planning phase of a wind power plant (WPP) project. This facilitates proper allocation of passive filters and reduces risk of non-compliance of the WPP with harmonic emission limits. Electromagnetic transient (EMT) models can be used to calculate harmonic emissions in WPPs but have restrictively long simulation times when multiple wind turbine model instances are required. This precludes EMT modeling of WPPs consisting of tens to hundreds of wind turbines, instead linear harmonic models are often used.

The simplest and most widely used method for linear harmonic modeling wind turbines utilizes harmonic current sources. Harmonic current sources have been used to compute harmonic flows in DFIG based wind farms [2], applied to the calculation of aggregated current harmonics in a wind farm connected to a public grid [3], used to assess the accuracy of collector system models [4] and as a basis for probabilistic modeling of wind turbine harmonic sources [5]. In addition, harmonic current sources form the basis for harmonic assessment of wind turbines in IEC 61400-21:2008 [6]. Unfortunately, PQ computations based on current source models can be misleading due to a misrepresentation of the internal harmonic source of the converter [1],[7]-[10]. Consequently, a per-phase converter harmonic model of the grid-side voltage-source converter (VSC) of a Type-IV wind turbine was proposed [9] and extended in [11] to a sequence domain (SD) harmonic model where the three-phase properties of the converter are maintained.

A challenge when using linear models to compute harmonic emissions by a WPP is assigning the phase of each harmonic source (wind turbine) to achieve the correct aggregated harmonic voltages and currents at the PCC. This is important because it is the harmonics at the PCC that are checked for compliance with harmonic emission limits. The classic approach for aggregating power systems harmonics assumes uniformly distributed magnitude and phase of the constituent harmonic phasors [12],[13] giving closed-form solutions for the probability density functions (PDFs) of the aggregated harmonic phasor. On the contrary, the phase of converter generated low-order characteristic odd voltage harmonics due to dead-time [14]-[17] have been shown to depend deterministically on the phase of the fundamental component of converter current [11].

In this paper a probabilistic SD harmonic model is employed for calculating harmonic emissions by WPPs comprised of Type-IV wind turbines. The following claims are made:

1) The SD harmonic model, see Section II-A, can be used to integrate converter generated voltage harmonics of both deterministic and probabilistic basis.
2) The SD representation naturally partitions converter generated voltage harmonics into two groups; a deterministic group, see Section II-B and a probabilistic group, see Section II-C.
3) The aggregated SD voltages and currents can be expressed as a per-phase magnitude distribution, see Section II-D.

Section III reports a case study on a fictitious WPP consisting of ten string-connected, $3MW$, Type-IV wind turbines. Results from a PSCAD implementation of the WPP are compared to the corresponding probabilistic SD harmonic model under different resonance conditions and wind turbine operating points. The probabilistic SD harmonic model can be employed in the planning phase of WPP projects to assess harmonic emissions to a given quantile, potentially avoiding an over-engineering of passive filters otherwise needed to satisfy infrequently occurring cases.

II. Harmonic Modeling Methods

Fig. 1 shows a fictitious WPP consisting of N string-connected Type-IV wind turbines. Each wind turbine's grid-side VSC is coupled to the collector system through a filter inductor L. The step-up transformers, interconnecting cables, bulk transmission cable and lumped grid are denoted by their rated impedance Z_{TX}, Z_L, Z_{LG} and Z_g respectively[1].

[1]For brevity the PWM filters and cable shunt capacitors have been omitted from Fig. 1.

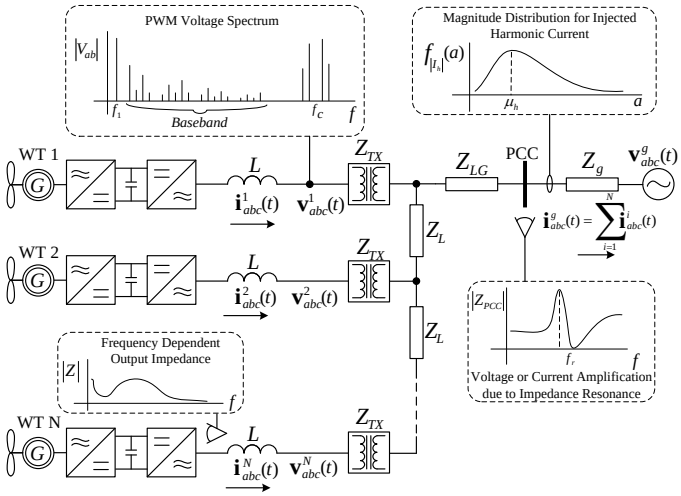

Fig. 1: Fictitious WPP consisting of N string-connected, Type-IV wind turbines connected to an external grid.

A. Sequence Domain Harmonic Model

A block diagram of the ith grid-side VSC, $i = 1, ..., N$, is shown in Fig. 2. The time-domain vectors, $\mathbf{i}^i_{abc}(t)$ and $\mathbf{v}^i_{abc}(t)$, represent the phase currents and phase-ground voltages at the grid-side of the filter inductor L respectively. The SD harmonic

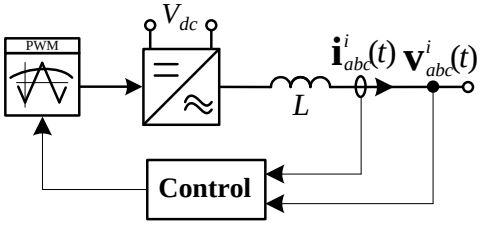

Fig. 2: Block diagram of a grid-side VSC used in a Type-IV wind turbine.

model of the VSC [11] is developed in the frequency domain as

$$\mathbf{v}^{d,i}_{pn}(jh\omega_1) = \mathbf{Z}_{pn}\mathbf{i}^i_{pn}(jh\omega_1) + \mathbf{v}^i_{pn}(jh\omega_1) \tag{1}$$

where $\mathbf{i}^i_{pn}(jh\omega_1)$ and $\mathbf{v}^i_{pn}(jh\omega_1)$ are the SD counterparts of $\mathbf{i}^i_{abc}(t)$ and $\mathbf{v}^i_{abc}(t)$ respectively calculated at each harmonic order, h, of the fundamental frequency, ω_1. The closed-loop control of the converter is captured in the SD impedance matrix $\mathbf{Z}_{pn}$ which can be derived analytically [19] or extracted numerically [20]. $\mathbf{v}^{d,i}_{pn}(jh\omega_1)$ is the vector of *apparent* harmonic voltage sources generated by the converter. Each instance of $\mathbf{v}^{d,i}_{pn}(jh\omega_1)$ is valid for the operating point (active power injection) under which it was calculated. An instance of $\mathbf{v}^{d,i}_{pn}(jh\omega_1)$ can be calculated from real measurements on the wind turbine in question [9] or from a corresponding electromagnetic transient (EMT) model [11]. Under balanced and slightly unbalanced grid conditions $\mathbf{Z}_{pn}$ is approximately diagonal [19] such that

$$\mathbf{v}^{d,i}_{pn}(jh\omega_1) = \begin{bmatrix} Z_{pp}(jh\omega_1) & 0 \\ 0 & Z_{nn}(jh\omega_1) \end{bmatrix} \mathbf{i}^i_{pn}(jh\omega_1) + \mathbf{v}^i_{pn}(jh\omega_1) \tag{2}$$

which equates to two decoupled Thevenin equivalent circuits. The WPP model shown in Fig. 1 is transformed into the frequency domain by substituting an instance of the SD harmonic model for each wind turbine as shown in Fig. 3. The transformers, cables and external grid are modeled by their SD impedance matrix calculated at each harmonic order[2].

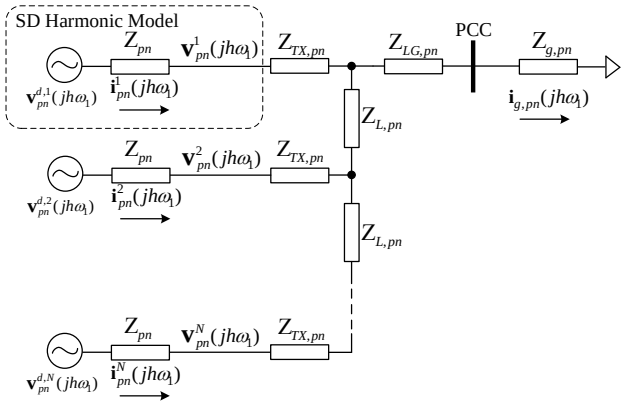

Fig. 3: Linear harmonic model of the WPP with an instance of the SD harmonic model for each wind turbine VSC.

B. Characteristic Converter Generated Voltage Harmonics

The apparent harmonic voltage source, $\mathbf{v}^{d,i}_{pn}(jh\omega_1)$, is comprised of harmonic sources with different phase and magnitude characteristics. Within the linear modulating range, low-order converter generated voltage harmonics ($f \leq f_c/2$) are predominately contributed by dead-time error pulses [14],[15]. In high-power applications the dead-time delay, T_d, is typically in the range of $1\% - 3\%$ of the switching period, T_c.

Both uncompensated dead-time (UDT) and compensated dead-time (CDT) schemes are used in grid-connected VSCs. Under UDT and sinusoidal load currents the averaged error pulses form a square wave of height DV_{dc}, $D = T_d/T_c$, and opposite polarity to the load current [15]-[17]. Multiple zero-crossings in the load current have been shown to eliminate some of the error pulses in the vicinity of the fundamental current zero-crossing [17]. Let $k_d \in \mathbb{N}$ represent the number of misplaced error pulses that occur each side of the fundamental current zero-crossing. The averaged a-phase to DC mid-point error pulse voltage, $\bar{e}_{a,UDT}(t)$, with respect to the zero-crossing of the a-phase fundamental component of current, $i_{a,1}(t)$, is shown in Fig. 4a and has Fourier coefficients

$$E_{h,UDT} = \frac{2V_{dc}D}{h\pi}\cos\left(k_d\frac{2\pi h}{p}\right)e^{jh\theta_1}. \tag{3}$$

θ_1 is the phase of the fundamental component of current, h is an odd harmonic order and $p = \omega_c/\omega_1$ is the pulse ratio.

[2]Of interest are the aggregated harmonics due to the harmonic sources within the wind farm so the grid model appears as an impedance only.

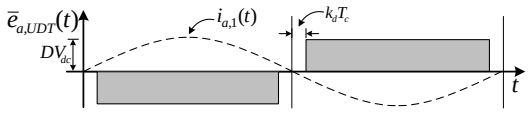

(a) Averaged error pulse signal, $\bar{e}_{a,UDT}(t)$, due to UDT.

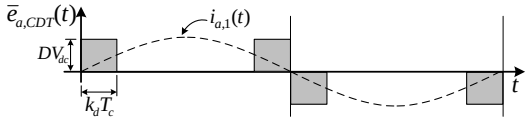

(b) Averaged error pulse signal, $\bar{e}_{a,CDT}(t)$, due to CDT.

Fig. 4: Averaged error pulse voltage due to dead-time and multiple zero-crossings in the load current.

Compensated dead-time (CDT) schemes delay or advance the active switching edge depending on the polarity of the sampled load current [15],[16], avoiding most of the error pulses. Under CDT, multiple zero crossings in the load current can cause error pulses in the vicinity of the fundamental current zero-crossing [11]. The averaged error pulse voltage $\bar{e}_{a,CDT}(t)$ is shown in Fig. 4b and has Fourier coefficients

$$E_{h,CDT} = \frac{2V_{dc}D}{h\pi}\left[1-\cos\left(k_d\frac{2\pi h}{p}\right)\right]e^{jh\theta_1}. \quad (4)$$

Balanced three-phase fundamental load currents will generate balanced three-phase load voltages, $\bar{\mathbf{e}}_{abc}(t)$, due to the averaged error pulses. The SD Fourier series representation of $\bar{\mathbf{e}}_{abc}(t)$ is

$$\bar{\mathbf{e}}_{pn}(t) = \sum_{h=-\infty}^{\infty}\frac{E_h}{3}\begin{bmatrix}1+2\cos(\frac{2\pi}{3}(h-1))\\ 1+2\cos(\frac{2\pi}{3}(h+1))\end{bmatrix}e^{jh\omega_1 t}. \quad (5)$$

where E_h are the Fourier coefficients of the a-phase to DC mid-point error pulse voltage ($\bar{e}_{a,UDT}(t)$ for example). Equation (5) depicts the *characteristic* spectrum of six-pulse converters where all non-zero positive and negative sequence odd harmonics are of the order $h = 6k+1$ and $h = 6k-1$ respectively, where $k \in \mathbb{N}$. Consequently, error pulses due to dead-time schemes also produce characteristic voltage harmonics with phase linearly related to the phase of the fundamental component of current, θ_1. Conveniently, this means a load flow can be employed to calculate θ_1^i for the ith wind turbine in a WPP containing N wind turbines. The phase of the hth characteristic harmonic used in the SD harmonic model is then calculated *deterministically* as $h\theta_1^i$. For example $\arg(v_n^{d,i}(j5\omega_1)) = 5\theta_1^i$ and $\arg(v_p^{d,i}(j7\omega_1)) = 7\theta_1^i$.

C. Carrier Sideband and Non-characteristic Converter Generated Voltage Harmonics

Carrier sideband voltage harmonics generated by carrier-based PWM schemes are defined by the modulation scheme and the fundamental component in the modulating signal [21]. The phase of carrier sideband harmonics are proportional to the phase of the PWM carrier, ϕ_c. The sampling by the ith wind turbine VSC in a WPP is random hence ϕ_c^i is a random variable with circular uniform distribution $\mathcal{U}(0, 2\pi)$.

The *non-characteristic* spectrum of harmonics includes the even harmonics, triplen harmonics and the odd positive and negative sequence harmonics of order $h = 6k-1$ and $h = 6k+1$ respectively, where $k \in \mathbb{N}$. In Type-IV wind turbines the generation of non-characteristic harmonics is largely attributed to asymmetry in the dead-time error pulses, non-linearity of the switching devices and semi-conductor voltage drops. These factors combine such that the phase of non-characteristic harmonics appears random. In lieu of a precise understanding of the phase distribution of non-characteristic harmonics the distribution with maximal entropy is chosen [22]. The circular uniform distribution $\mathcal{U}(0, 2\pi)$ has maximal entropy for the class of circular distributions, thereby minimizing the amount of prior information. Another motivating factor for choosing $\mathcal{U}(0, 2\pi)$ to represent the phase of non-characteristic harmonics is that physical systems often transition to maximal entropy configurations over time (principle of maximum entropy).

D. Magnitude Distribution of Sums of Harmonic Phasors

Let the sum of positive sequence current phasors (with harmonic order h) at the PCC of a WPP due to N harmonic sources (wind turbines) be $I_{p,h}$ where

$$I_{p,h} = |I_{p,h}|e^{i\theta_{p,h}} = X_{p,h} + jY_{p,h} = \sum_{i=1}^{N}(X_{p,h}^i + jY_{p,h}^i). \quad (6)$$

Suppose the constituent harmonic phasors $I_{p,h}^i = X_{p,h}^i + jY_{p,h}^i$ have real and imaginary parts with zero-mean and variance $(\sigma_{p,h}^i)^2$. The central limit theorem is generally satisfied for large N if the variance of the sum $\sigma_{p,h}^2 = \sum_{i=1}^{N}(\sigma_{p,h}^i)^2$ is not dominated by a single term [23]. This permits individual phasors being non-identically distributed but the sum of phasors being approximately bivariate normally distributed [12],[13]. The joint PDF for the sum of positive sequence harmonic phasors is

$$f_{X_{p,h},Y_{p,h}}(x,y) = \frac{1}{2\pi\sigma_{p,h}^2}e^{-\frac{1}{2\sigma_{p,h}^2}\left[x^2+y^2\right]} \quad (7)$$

where $X_{p,h}$ and $Y_{p,h}$ are normally distributed as $\mathcal{N}(0, \sigma_{p,h}^2)$. Converting (7) to polar coordinates and finding the marginal distribution of the magnitude $|I_{p,h}|$ gives the Rayleigh distribution $\mathcal{R}(\sigma_{p,h}^2)$ with PDF

$$f_{|I_{p,h}|}(a) = \frac{a}{\sigma_{p,h}^2}e^{-\frac{a^2}{2\sigma_{p,h}^2}}. \quad (8)$$

If the center of the joint PDF is offset from zero due to a constant factor then

$$f_{X_{p,h},Y_{p,h}}(x,y) = \frac{1}{2\pi\sigma_{p,h}^2}e^{-\frac{1}{2\sigma_{p,h}^2}\left[(x-\mu_{px,h})^2+(y-\mu_{py,h})^2\right]}. \quad (9)$$

The mean of the real and imaginary parts of $I_{p,h}$ are $\mu_{px,h} = \sum_{i=1}^{N}\mu_{px,h}^i$ and $\mu_{py,h} = \sum_{i=1}^{N}\mu_{py,h}^i$ respectively. The distance between the origin and the center of the joint PDF is $d_h^2 = \mu_{px,h}^2 + \mu_{py,h}^2$ [23]. The marginal distribution of

the magnitude of (9) is the Rice distribution $\mathcal{S}(d_h, \sigma^2_{p,h})$ with PDF

$$f_{|I_{p,h}|}(a) = \frac{a}{\sigma^2_{p,h}} e^{-\frac{1}{2\sigma^2_{p,h}}(a^2+d_h^2)} I_0\left(\frac{a d_h}{\sigma^2_{p,h}}\right). \quad (10)$$

Analogous expressions for (6)-(10) exist for the sum of negative sequence harmonic current phasors $I_{n,h}$. An example of $\mathcal{R}(\sigma^2)$ and $\mathcal{S}(d, \sigma^2)$ is shown in Fig. 5 for $\sigma^2 = 1$ and $d = 3$.

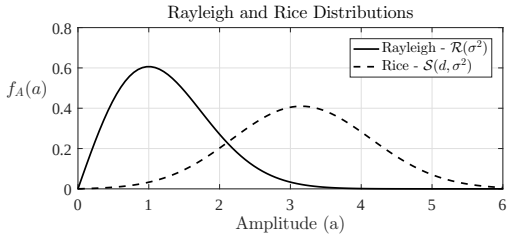

Fig. 5: Rayleigh and Rice distributions when $\sigma^2 = 1$ and $d = 3$.

$I_{p,h}$ and $I_{n,h}$ are converted to phase components as

$$\begin{bmatrix} I_{a,h} \\ I_{b,h} \\ I_{c,h} \end{bmatrix} = \begin{bmatrix} 1 & 1 \\ \alpha^2 & \alpha \\ \alpha & \alpha^2 \end{bmatrix} \begin{bmatrix} I_{p,h} \\ I_{n,h} \end{bmatrix} \quad (11)$$

which for the a-phase gives

$$I_{a,h} = X_{p,h} + X_{n,h} + j(Y_{p,h} + Y_{n,h}). \quad (12)$$

If $I_{p,h}$ and $I_{n,h}$ are independent then the sum of random variables $X_{p,h} + X_{n,h}$ and $Y_{p,h} + Y_{n,h}$ are normally distributed as $\mathcal{N}(0, \sigma^2_{p,h} + \sigma^2_{n,h})$ giving $|I_{a,h}| \sim \mathcal{R}(\sigma^2_{p,h} + \sigma^2_{n,h})$. Using basic properties of the normal distribution it can be shown that $|I_{b,h}|$ and $|I_{c,h}|$ are also Rayleigh distributed as $\mathcal{R}(\sigma^2_{p,h} + \sigma^2_{n,h})$. It is a remarkable that under certain conditions a per-phase magnitude distribution denoted $|I_{x,h}|$ where $x = a, b, c$ contains the information about both the positive and negative sequence components. This is fortuitous as harmonic emission standards typically quote emission limits in terms of per-phase values [24],[25].

The magnitude distribution $|I_{x,h}| \sim \mathcal{R}(\sigma^2_{p,h} + \sigma^2_{n,h})$ is applicable when the positive and negative sequence harmonic sources are both of non-characteristic type as discussed in Section II-C. If either $I_{p,h}$ or $I_{n,h}$ arise from characteristic type harmonic sources, as discussed in Section II-B, then a deterministic factor d_h must be added and $|I_{x,h}|$ becomes Rice distributed as $\mathcal{S}(d_h, \sigma^2_{p,h} + \sigma^2_{n,h})$. An example is the 5th harmonic currents which are comprised of a deterministic $I_{n,5}$ and a probabilistic $I_{p,5}$. In summary the magnitude distributions for the sum of harmonic currents injected by a WPP consisting of Type-IV wind turbines are categorized as

$$|I_{x,h}| \sim \begin{cases} \mathcal{R}(\sigma^2_{p,h} + \sigma^2_{n,h}) & \text{even, triplen, carrier sideband} \\ \mathcal{S}(d_h, \sigma^2_{p,h} + \sigma^2_{n,h}) & \text{odd (non-triplen).} \end{cases} \quad (13)$$

E. Monte-Carlo Methods

Monte-Carlo methods provide numerical solutions to problems that lack closed-form solutions or are non-deterministic. In crude Monte-Carlo simulations the random variables and inputs draw from designated distributions giving an error in the output variance proportional to $1\sqrt{n}$ where n is the number of samples [18]. Therefore, four times the number of samples are generally needed to halve the error.

Normally when assessing harmonic emissions only a measure of the sampled output quantities is required. The 95th-quantile of the magnitude is a commonly used measure as it includes the region of the sample space with the highest probability but avoids the tail of the PDF. This avoids over engineering remedial solutions for cases that occur infrequently. The 95th-quantile of a Rayleigh distribution is actually the basis for the summation factor for harmonics of order $h > 10$ found in IEC 61000-3-6 [24]. Suppose a quantile is desired for the non-characteristic harmonics. The z-th quantile $Q_{\mathcal{R}}(z)$ for the Rayleigh distribution $|I_{x,h}| \sim \mathcal{R}(\sigma^2_{p,h} + \sigma^2_{n,h})$ is

$$Q_{\mathcal{R}}(z) = \sigma\sqrt{-2\ln(1-z)} \quad (14)$$

which for $\sigma^2 = \sigma^2_{p,h} + \sigma^2_{n,h}$ and $z = 0.95$ gives

$$Q_{\mathcal{R}}(0.95) \approx \sqrt{6(\sigma^2_{p,h} + \sigma^2_{n,h})}. \quad (15)$$

Therefore, the 95th-quantile of $|I_{x,h}|$ is calculated directly based on the sample variances of $\sigma^2_{p,h}$ and $\sigma^2_{n,h}$ obtained by the Monte-Carlo simulation. For characteristic harmonics either the positive or negative sequence component has a deterministic offset d_h. The z-the quantile of the Rice distribution $Q_{\mathcal{S}}(z)$ is well approximated by the normal distribution when $d/\sigma \gg 3$ [23] such that

$$Q_{\mathcal{S}}(z) \approx d + \sigma\sqrt{2} \cdot \text{erf}^{-1}(2z - 1) \quad (16)$$

which for $z = 0.95$, $d^2 = \mu^2_{X,h} + \mu^2_{Y,h}$ and $\sigma^2 = \sigma^2_{p,h} + \sigma^2_{n,h}$ gives

$$Q_{\mathcal{S}}(0.95) \approx \sqrt{\mu^2_{X,h} + \mu^2_{Y,h}} + 1.645 \cdot \sqrt{\sigma^2_{p,h} + \sigma^2_{n,h}}. \quad (17)$$

III. Case Study

The WPP shown in Fig. 1 was implemented in PSCAD as a means of evaluating the probabilistic SD harmonic modeling method. The WPP consisted of a string of $N = 10$, $3MW$, Type-IV wind turbines with the ratings given in Table I. Each wind turbine instance contained a reduced-order mechanical model, a switched converter model (including dead-time placement and compensation) and the control software implementation. Two instances of the PSCAD model were simulated for each case: first, $\phi^i_c = 0$ so that sampling by each wind turbine VSC was synchronized (approximate worst case); second, $\phi^i_c \sim \mathcal{U}(0, 2\pi)$ so sampling by each wind turbine VSC was random. The lumped grid model had a short-circuit and X/R ratio of 5. The interconnecting cables Z_L were modeled as PI equivalents of a typical three-phase underground cable of $1000m$ length. The bulk transmission cable Z_{LG} was similarly modeled but had variable length

depending on the case.

TABLE I: Ratings of the Type-IV wind turbine grid-side VSC.

Parameter	Value
Rated Active Power	3 MW
Grid Frequency	50 Hz
Rated Voltage (line-line)	690 V_{RMS}
Switching Frequency	2.5 kHz
Dead-time Delay	4 μs
Dead-time Scheme	CDT

A crude Monte-Carlo simulation was used to implement the probabilistic SD harmonic models of the wind turbines. The magnitude of the apparent harmonic voltage sources $\mathbf{v}_{pn}^{d,i}(jh\omega_1)$, $i = 1, ..., N$, for the particular Type-IV wind turbine used in the WPP were initially determined at each operating point (active power injection) [11]. The phase of $\mathbf{v}_{pn}^{d,i}(jh\omega_1)$ was assigned according to Sections II-B and II-C. The positive and negative sequence linear models were then solved to obtain $|V_{x,h}|$ and $|I_{x,h}|$ at the PCC of the WPP. The Monte-Carlo simulation generated $n = 500$ samples at each harmonic order h.

A. Mixed Operating Points - Short Length Cable

Turbines 1-3, 4-6 and 6-10 injected 80%, 50% and 20% of rated active power respectively and Z_{LG} was based on a $10km$ long cable. Fig. 6 shows $|V_{x,h}|$ and $|I_{x,h}|$ compared to the PSCAD results. The characteristic odd harmonics exhibit negligible in magnitude when $\phi_c^i = 0$ or $\phi_c^i \sim \mathcal{U}(0, 2\pi)$. Conversely, Fig. 7 shows that $\phi_c^i \sim \mathcal{U}(0, 2\pi)$ affected the switching sideband harmonics as they were largely canceled at the PCC (for that particular random instance of ϕ_c^i). The 95th-quantile of the switching sideband harmonics was just over 50% of the synchronized value which agrees with the theoretical value[3].

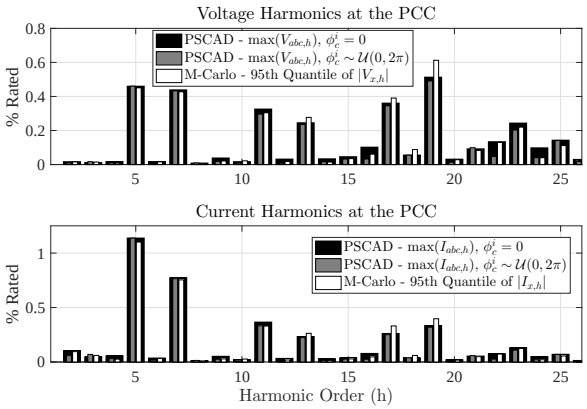

Fig. 6: Baseband harmonics at the PCC when the wind turbines are injecting different levels of active power.

[3]Given N phasors with constant amplitude A and uniformly distributed phase the 95th-quantile of the aggregated sum attenuates as $\sqrt{3/N}$.

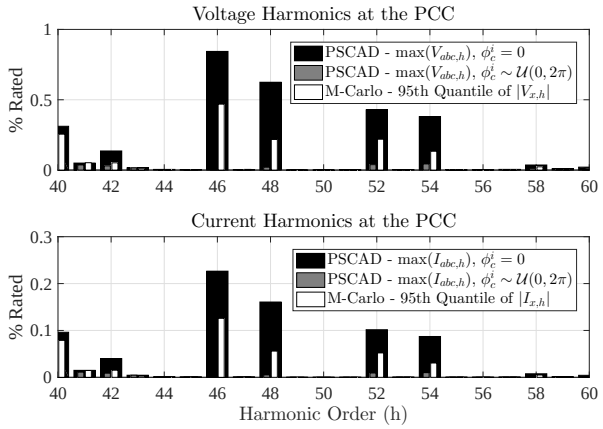

Fig. 7: Switching sideband harmonics at the PCC when the wind turbines are injecting different levels of active power.

B. Same Operating Points - Medium Length Cable

All turbines injected 100% rated active power, Z_{LG} was based on a $30km$ long cable and a resonance occurred at 30th harmonic. Fig. 8 shows that the magnitude of the amplified harmonic current $|I_{x,30}|$ is largely reduced in when $\phi_c^i \sim \mathcal{U}(0, 2\pi)$, which is reflected in the corresponding 95th-quantile obtained by the Monte-Carlo simulation. This highlights how random sampling amongst wind turbines naturally attenuates the aggregated non-characteristic harmonics.

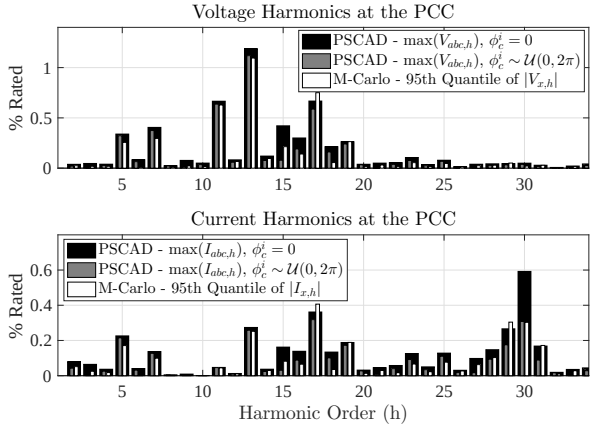

Fig. 8: Baseband harmonics at the PCC when a resonance occurs around the 30th harmonic.

C. Same Operating Points - Long Length Cable

All turbines injected 100% rated active power, Z_{LG} was based on a $50km$ long cable and a resonance occurred near the 11th harmonic. Fig. 9 shows that the amplified characteristic harmonic exhibits little attenuation when $\phi_c^i \sim \mathcal{U}(0, 2\pi)$. The probabilistic SD harmonic model captures to a large degree the resonance seen in the PSCAD model. This is critical for the efficacy of a harmonic model used in the planning phase of a new WPP.

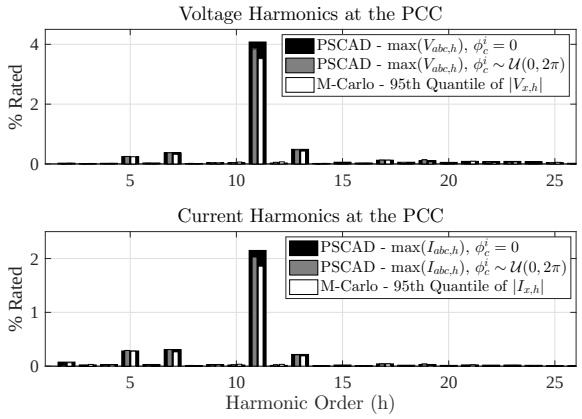

Fig. 9: Baseband harmonics at the PCC when a resonance occurs around the 11th harmonic.

IV. Conclusion

This paper has shown how a probabilistic SD harmonic model of a grid-connected VSC can be used to estimate harmonic emissions due to WPPs comprised of Type-IV wind turbines. The SD representation naturally partitioned converter generated voltage harmonics into two groups; those with deterministic phase or those with probabilistic phase. The phase of deterministic harmonics are assigned through load flow. The phase of probabilistic harmonics are drawn from a circular uniform distribution. A per-phase quantile is calculated from the aggregated SD quantities for direct comparison to stipulated harmonic emission limits.

A fictitious WPP consisting of ten string-connected, $3MW$, Type-IV wind turbines was used to evaluate the probabilistic SD harmonic model. The 95th-quantile of the aggregated harmonic voltages and currents generated by a Monte-Carlo simulation were compared to the corresponding results obtained by a PSCAD model. The probabilistic SD harmonic model replicated the harmonic response of the WPP obtained by PSCAD for different resonance conditions and wind turbine operating points. The probabilistic SD harmonic model can be used in the planning phase of WPP projects to estimate harmonic emissions to a given quantile, potentially avoiding an over-engineering of passive filters otherwise needed to satisfy infrequently occurring cases.

Future Work

The Monte-Carlo framework can be extended to include other random factors. For example, the wind turbine operating point could be made a random variable. The aggregated harmonic voltages and currents at the PCC would then include information about the time-varying nature of the energy sources.

Acknowledgment

This work was supported by Siemens Gamesa Renewable Energy A/S and the Innovations Fund, Denmark.

References

[1] J. Arrillaga and N. R. Watson, "Power System Harmonics," John Wiley & Sons Inc., Hoboken, NJ, USA, 2003.

[2] S. A. Papathanassiou and M. P. Papadopoulos, "Harmonic Analysis in a Power System with Wind Generation," IEEE Transactions on Power Delivery, vol. 21, no. 4, pp. 2006–2016, Oct. 2006.

[3] K. Yang, et al., "Aggregation and Amplification of Wind-Turbine Harmonic Emission in a Wind Park," IEEE Transactions on Power Delivery, vol. 30, no. 2, pp. 791–799, Apr. 2015.

[4] F. Ghassemi and K.-L. Koo, "Equivalent Network for Wind Farm Harmonic Assessments," IEEE Transactions on Power Delivery, vol. 25, no. 3, pp. 1808–1815, Jul. 2010.

[5] Y. Cho, et al., "A Framework to Analyze the Stochastic Harmonics and Resonance of Wind Energy Grid Interconnection," Energies, no. 9: 700, 2016.

[6] "Wind Turbines – Part 21: Measurement and Assessment of Power Quality Characteristics of Grid Connected Wind Turbines," International Electrotechnical Commission Standard IEC-61400-21, 2008.

[7] K. Yang, et al., "Decompositions of Harmonic Propagation in Wind Power Plant," Electric Power Systems Research, vol. 141, pp. 84–90, Dec. 2016.

[8] Ł. H. Kocewiak, et al., "Wind Turbine Harmonic Model and Its Application – Overview, Status and Outline of the New IEC Technical Report," in the 14th Wind Integration Workshop, Brussels, October 2015.

[9] P. Brogan and N. Goldenbaum, "Harmonic Model of the Network Bridge Power Converter for Wind Turbine Harmonic Studies," in The 11th Wind Integration Workshop, Lisbon, 2012.

[10] L. Shuai, L. H. Kocewiak and K. H. Jensen, "Application of Type 4 Wind Turbine Harmonic Model for Wind Power Plant Harmonic Study," in The 15th Wind Integration Workshop, Vienna, 2016.

[11] E. Guest, K. H. Jensen, and T. W. Rasmussen "Sequence Domain Harmonic Modeling of Type-IV Wind Turbines," IEEE Transactions on Power Electronics, *Preprint*, no. 99, Aug. 2017.

[12] W. E. Kazibwe, T. H. Ortmeyer and M. S. A. A. Hammam, "Summation of Probabilistic Harmonic Vectors," IEEE Transactions on Power Delivery, vol. 4, no. 1, pp. 621–628, Jan. 1989.

[13] M. Lehtonen, "A General Solution to the Harmonics Summation Problem," European Transactions on Electric Power, vol. 3, no. 3, pp. 293–297, July 1993.

[14] C. D. Townsend, G. Mirzaeva, and G. C. Goodwin, "Deadtime Compensation for Model Predictive Control of Power Inverters," IEEE Transactions on Power Electronics, vol. 32, no. 9, pp. 7325–7337, Sep. 2017.

[15] D. Leggate and R.J. Kerkman, "Pulse-Based Dead-Time Compensator for PWM Voltage Inverters," IEEE Transactions on Industrial Electronics, vol. 44, no. 2, pp. 191–197, 1997.

[16] S.-G. Jeong and M.-H. Park, "The Analysis and Compensation of Dead-Time Effects in PWM Inverters," IEEE Transactions on Industrial Electronics, vol. 38, no. 2, pp. 108–114, 1991.

[17] G. Grandi, et al., "Effects of Current Ripple on Dead-Time Distortion in Three-phase Voltage Source Inverters," 2012 IEEE Energy Conference and Exhibition (ENERGYCON), 2012, pp. 207–212.

[18] J. M. Hammersley and D. C. Handscomb, "Monographs on Applied Probability and Statistics: Monte Carlo Methods," Chapman and Hall, London, GB, 1964.

[19] M. Cespedes and Jian Sun, "Impedance Modeling and Analysis of Grid-Connected Voltage-Source Converters," IEEE Transactions on Power Electronics, vol. 29, no. 3, pp. 1254–1261, Mar. 2014.

[20] M. Cespedes and J. Sun, "Three-phase impedance measurement for system stability analysis," in Control and Modeling for Power Electronics (COMPEL), 2013 IEEE 14th Workshop on, 2013, pp. 1–6.

[21] D. G. Holmes and T. A. Lipo, "Pulse Width Modulation for Power Converters: Principles and Practice," Wiley-IEEE Press, Hoboken, NJ, USA, 2003.

[22] A. Papoulis and S. U. Pillai, "Probability, Random Variables and Stochastic Processes," McGraw Hill Education, New Delhi, India, 2002.

[23] P. Beckmann, "Statistical Distribution of the Amplitude and Phase of a Multiply Scattered Field," Journal of Research of the National Bureau of Standards, vol. 66D, no. 3, pp. 231–240, Dec. 1961.

[24] "Electromagnetic compatibility (EMC) - Part 3-6: Limits - Assessment of emission limits for the connection of distorting installations to MV, HV and EHV power systems," International Electrotechnical Commission Standard IEC-61000-3-6, 2008.

[25] "IEEE Recommended Practices and Requirements for Harmonic Control in Electrical Power Systems," IEEE Standard 519, 2014.